

Civil Engineering Journal

(E-ISSN: 2476-3055; ISSN: 2676-6957)

Vol. 11, No. 09, September, 2025



Impact-Echo Method on Short Cylinders: A Numerical and Experimental Investigation

Panagiotis Pelekis ¹, Vassilis G. Siorikis ^{2, 3}, Constantinos P. Antonopoulos ², Geraldo L. Osmani ¹, George D. Hatzigeorgiou ³

¹ Department of Civil Engineering, University of Patras, 26504 Patras, Greece.

² School of Pedagogical and Technological Education, Hellenic Open University, 14121 Athens, Greece.

³ School of Science and Technology, Hellenic Open University, 26331 Patras, Greece.

Received 03 April 2025; Revised 07 August 2025; Accepted 20 August 2025; Published 01 September 2025

Abstract

Despite the widespread use of Ultrasonic Pulse Velocity (UPV) to estimate the dynamic properties of materials, the accuracy of its results for concrete and rock cylinders, even though it does not depend on cylinder slenderness, is directly affected by the a priori assumption of a specific value of the Poisson's ratio (ν), which can lead to errors of up to 50% in the calculation of the dynamic modulus of elasticity (E_d). In contrast, the Impact Echo (IE) method allows the calculation of E_d without the need-to-know Poisson's ratio, with an error of approximately 2%, but its results are affected not only by the slenderness ratio (L/D) but also by the inertia effect and the mass of the sensor. In this study, both UPV and IE—longitudinal and torsional—tests were carried out on cylindrical steel and aluminium specimens for six different slenderness values and L/D values ranging from 1-5. The experimental results fully confirm the authors' proposed shape correction factor (SCF). A numerical analysis of short cylinders is conducted to examine how the mass of the accelerometer used on the IE affects the results. Specifically, aluminium and steel specimens with six different slenderness values were simulated via the finite element method (FEM) via experimental evaluation. Inertia and mass interactions significantly affect the results. Two new correction factors were proposed for steel and aluminium cylinders to address this issue, and three different combinations of NDTs were tested to find that the dynamic properties are very sensitive to these parameters. Poisson's ratio has been accurately calculated for steel and aluminium cylinders and can be calculated for concrete and rock cores by applying the proposed correction factors.

Keywords: Impact-Echo; Ultrasonic Pulse Velocity; Finite Element Method; Dynamic Poisson's Ratio; Dynamic Young's Modulus; Non-Destructive Testing; Acoustic Resonance.

1. Introduction

Non-Destructive Testing (NDT) is a cornerstone of modern civil engineering, offering numerous advantages in terms of time efficiency, cost-effectiveness, and sustainability. NDT techniques allow inspections to be performed at various stages of a project's lifecycle, such as during construction, regular maintenance, or retrofitting, without disrupting operations. This adaptability minimizes downtime and ensures that projects stay on schedule. Furthermore, the cost-effectiveness of NDT lies in its ability to detect defects or issues early, thus preventing costly repairs and replacements. Providing detailed data for informed decision-making reduces unnecessary expenditures on materials and labor. Additionally, because NDT methods are nonintrusive, structures can remain operational during inspections, which is particularly beneficial for large-scale infrastructure projects.

^{*} Corresponding author: vsiorikis@aspete.gr





© 2025 by the authors. Licensee C.E.J, Tehran, Iran. This article is an open access article distributed under the terms and conditions of the Creative Commons Attribution (CC-BY) license (http://creativecommons.org/licenses/by/4.0/).

From a safety perspective, NDT ensures compliance with regulations by identifying structural defects such as cracks, voids, or corrosion that could compromise integrity. Addressing these issues proactively leads to safer environments for both workers and occupants while reducing liability risks for stakeholders. Moreover, the non-destructive nature of these methods aligns with sustainable practices, as they generate no waste and preserve resources. In an era where balancing progress with environmental considerations is critical, NDT contributes to more sustainable construction practices. Overall, non-destructive testing is indispensable in civil engineering, saving time, cutting costs, and ensuring the quality and safety of modern infrastructure.

1.1. Ultrasonic Pulse Velocity Method

One of the most commonly used NDT methods in civil engineering works is the UPV method. Its application varies and is very useful, especially in rock mechanics and in concrete construction, where through the calculation of dynamic elastic moduli, the compressive strength of rock and concrete can be calculated. Owing to its ease of use and low-cost equipment, the UPV method is very popular and is the most utilized NDT method. A schematic diagram of the method can be found in Figure 1. The fundamentals are described in ASTM C597, and the concept is that by measuring the time that a longitudinal ultrasonic pulse takes to travel through a medium, one can calculate the pulse velocity [1]. When the material density is known, the constrained or P-wave modulus (M) can be calculated as shown in Equation 1:

$$M = \rho \times V_p^2 \tag{1}$$

where V_p denotes the velocity of a P-wave and ρ denotes the density of the material through which the wave is propagating.

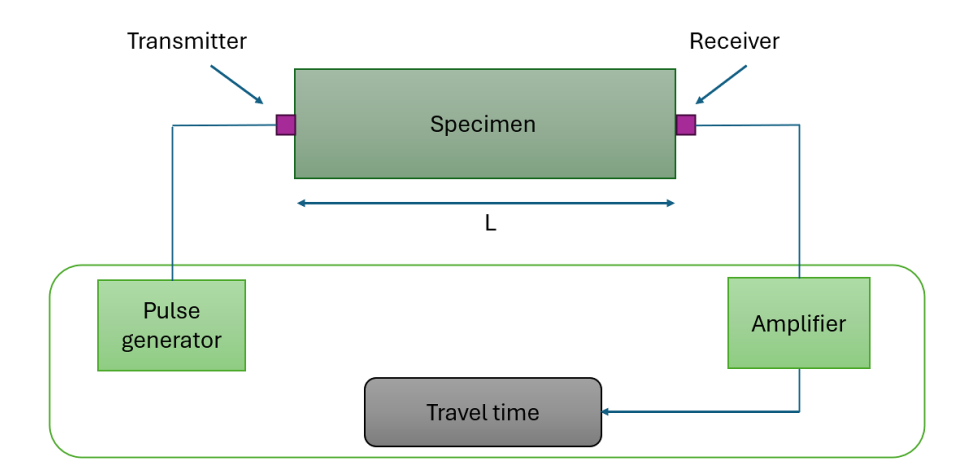


Figure 1. Schematic diagram of the UPV method

The constrained modulus is related to the dynamic Young's modulus (E_d) according to Equation 2. Poisson's ratio (v) acts as a correction factor and must be known in advance for the calculation. [2]

$$E_d = \frac{\rho \times V_p^2 \times (1+\nu) \times (1-2\nu)}{1-\nu}$$
 (2)

The UPV is broadly used in combination with either other NDT or destructive methods. The material property most strongly correlated with the UPV is the compressive strength. Many researchers have used empirical equations to estimate the compressive strength of concrete [2–6]. The interest in the research of the method is not diminishing. The well-established theoretical basis makes the application of the method easy and fast, with low-cost equipment. Recently, Choi et al. (2022) [7] used UPV to estimate the compressive and splitting tensile strengths of rubber concrete. All these empirical equations, when shown individually, have a very good correlation, but compared to each other, it is obvious that there is a large scatter in their results [8]. This is because it has a very serious drawback. Along with UPV readings, other parameters must be known or assumed. Espinosa et al. (2023) [9], in their research on self-compacting concrete with recycled aggregates, reported that the modulus elasticity can be estimated with a deviation of $\pm 10\%$ to $\pm 20\%$ on the basis of the known compressive strength of the samples. As seen in Equation 2, if Poisson's ratio (v) is not known, a value must be assumed to calculate the Young's modulus [10]. The error behind this assumption can be significant. In a previous study, our research team demonstrated an arbitrary assumption of Poisson's ratio. Figure 2 reported that this assumption can lead to an error ranging from 8.5% overestimation to 15.5% underestimation of the dynamic Young's modulus, whereas for a high value of Poisson's ratio of v= 0.40, the error can reach 50% underestimation [8].

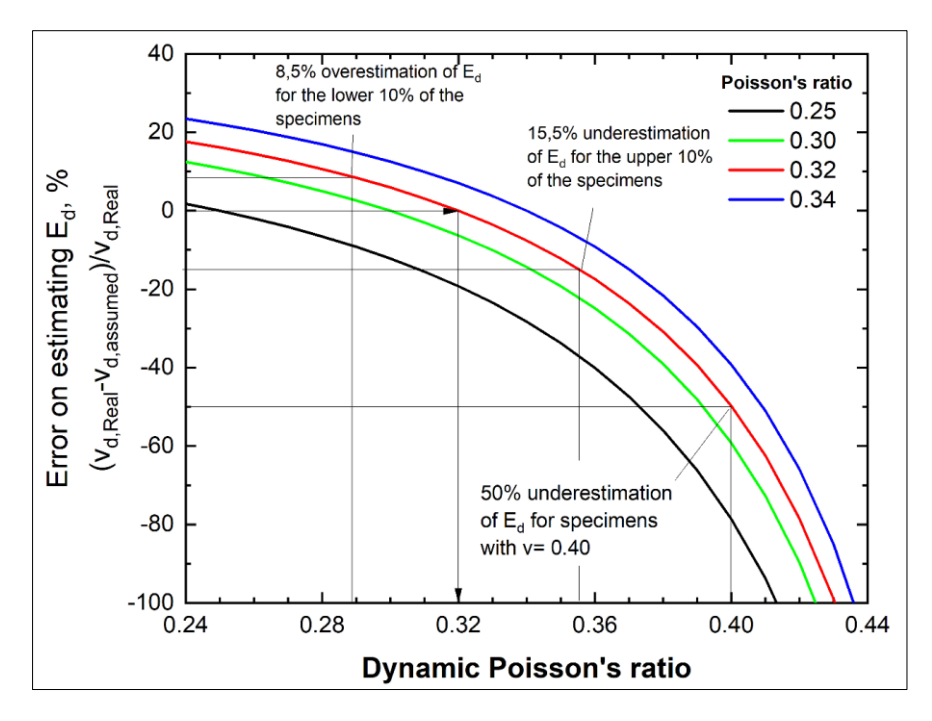


Figure 2. Error in the E_d estimation is associated with the selection of an arbitrary Poisson's ratio value [8]

1.2. Impact Echo Method

In contrast, the IE method does not require Poisson's ratio assumption from the beginning. This NDT method was developed and optimized by Professor Sansalone in 1983. It uses an inverse process to determine the dynamic properties of a material whose dimensions are known [11].

A lightweight accelerometer with a high enough frequency range is used to measure the specimen's response after a small object—typically a metallic sphere—impacts a supported sample. The surface motion is then recorded as a digital waveform in the time domain. This method has been increasingly investigated in recent years. Coleman and Schindler (2022) evaluated concrete bridge decks via three different NDT methods and discovered that the best way to assess the state of bridge decks was via IE [12]. The novel use of AI and machine learning has been used to analyze the results, yet recently, these methods have been applied. In addition to their typical application, Thurnherr et al. (2024) used drone-based impact-echo measurement sensors to apply the method to concrete structures that are difficult to inspect, such as bridges and piers [13]. Semi-supervised learning has been utilized to analyze and distinguish a large volume of IE test data measured at multiple points in a short period [14]. A similar approach to this study on FEM simulations of IE was used by Bahati et al. (2022), who reported how IE can be used to quantify and verify the depth and position of cavities in concrete slabs [15].

The popular fast Fourier transform (FFT) algorithm is used to translate these waveforms to the frequency domain. The spectrum peaks can be utilized to determine the wave velocity and assess the dynamic characteristics and structural integrity of materials [16]. From Equation 3, it becomes apparent that the Poisson's ratio value does not need to be known to calculate E_d . Moreover, the dynamic shear modulus (G_d) can be calculated via Equation 4. A schematic diagram of the method is presented in Figure 3.

$$E_d = \rho \cdot V_c^2 \tag{3}$$

$$G_d = \rho \cdot V_s^2 \tag{4}$$

where V_c and V_s are the longitudinal and torsional velocities, respectively, and ρ is the density of the material.

While it has been used by many researchers to determine the thickness and detect defects on plates and cylinders [16–23], yet this method does not come with no drawbacks. Accurately determining which peaks correspond to the resonant frequency is one of the difficulties with this approach. While Pandum et al. (2024) [24] employed artificial intelligence and deep learning methods to address this issue, Malone et al. (2023) [23] employed a multi-impact nonlinear analysis to discover fundamental IE frequencies [23, 24].

IE - Longitudinal mode

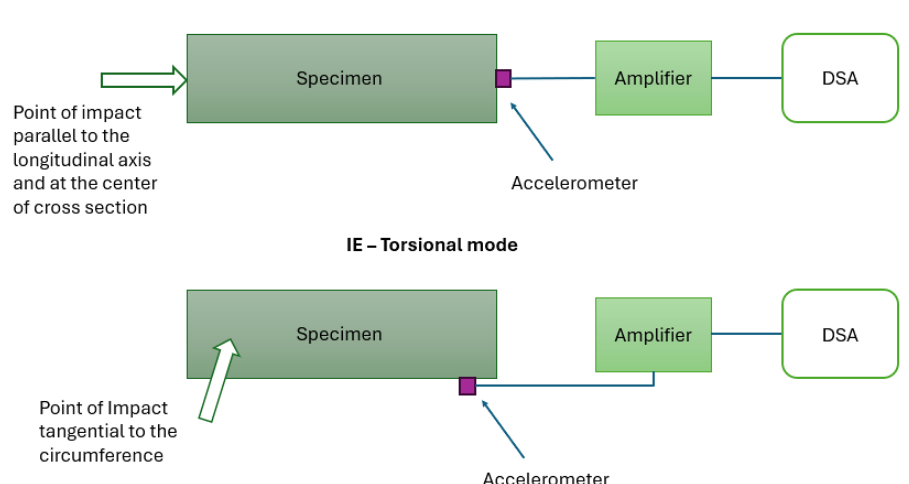


Figure 3. Schematic diagram of the IE method

The main issue, however, is that the measured resonant frequency depends on the slenderness of the sample and must be corrected. The shape correction factor (SCF) depends on Poisson's ratio, which reflects the need to know Poisson's ratio in advance. With a minimum slenderness ratio of two, according to ASTM C-215, the best outcomes are achieved when this ratio falls between three and five. This is because other vibration modes may interfere with the resonance frequency if the lateral dimensions are not five or six times larger than the dimensions parallel to the impact [25–27]. The dynamic Young's modulus and shear modulus (G_d) can be calculated via Equations 5 and 6, and the Poisson's ratio can be calculated via Equation 7 [11].

$$E_d = 5,093 \left(\frac{L}{D^2}\right) \cdot m \cdot f_c^2 \tag{5}$$

$$G_d = 4 \left(\frac{L \cdot R}{A}\right) \cdot m \cdot f_s^2 \tag{6}$$

$$v = \frac{E_d}{2G_d} - 1 \tag{7}$$

where L is the length and D is the diameter of the cylinder, R is the shape factor, m is the mass, A is the cross-sectional area of the test sample, and finally, f_c and f_s are the resonant longitudinal and torsional frequencies, respectively.

Owing to the slenderness effect, both the longitudinal and torsional frequencies must be corrected, whereas ASTM C-215 proposes a shape correction factor only for torsional frequencies, which for cylindrical samples is equal to 1. The majority of research has examined the impact of samples with L/D> 2.0. However, since this is the usual size of concrete cores drilled from existing structures, it is more helpful to acquire data for samples with L/D=1. The current calculation methods are insufficient to represent the IE implementation findings for small, short cylinders because they are fundamentally different from those for long cylinders. The measured frequencies need to be adjusted to account for the impact of L/D. Yao et al. (2022) also recognized the necessity for IE implementation correction and suggested Equation 8 for frequency correction [28].

$$f_{ie} = [(0.58L^{-1.01}) \cdot D - 0.060] \frac{0.92 \cdot C_p}{2D}$$
(8)

where f_{ie} denotes the frequency correction, L denotes the specimen length, D denotes the specimen diameter, and C_p denotes the wave propagation velocity.

Wang et al. (2012) and Siorikis et al. (2020, 2022, 2024) confirmed that there is a need to apply an SCF at the longitudinal frequency. The latter proposed the SCF of Equations 9 and 10, which results in a significantly smaller error than using only the UPV alone [8, 29–31]. In Figure 4, SCF versus slenderness L/D for six Poisson's ratio values is depicted.

$$y = y_0 + A_1 e^{-x/t_1} + A_2 e^{-x/t_2}$$
(9)

$$SCF = \frac{f_{Theoretical}}{f_{FEM}} \tag{10}$$

where y denotes the shape correction factor; x denotes the L/D ratio; and y_o , A_1 , A_2 , t_1 , and t_2 are coefficients that depend on Poisson's ratio. A combination of Equations 3 and 9 results in Equation 11.

$$V_c = (f_m \cdot SCF) \cdot 2L \tag{11}$$

where f_{m} denotes the measured resonant frequency.

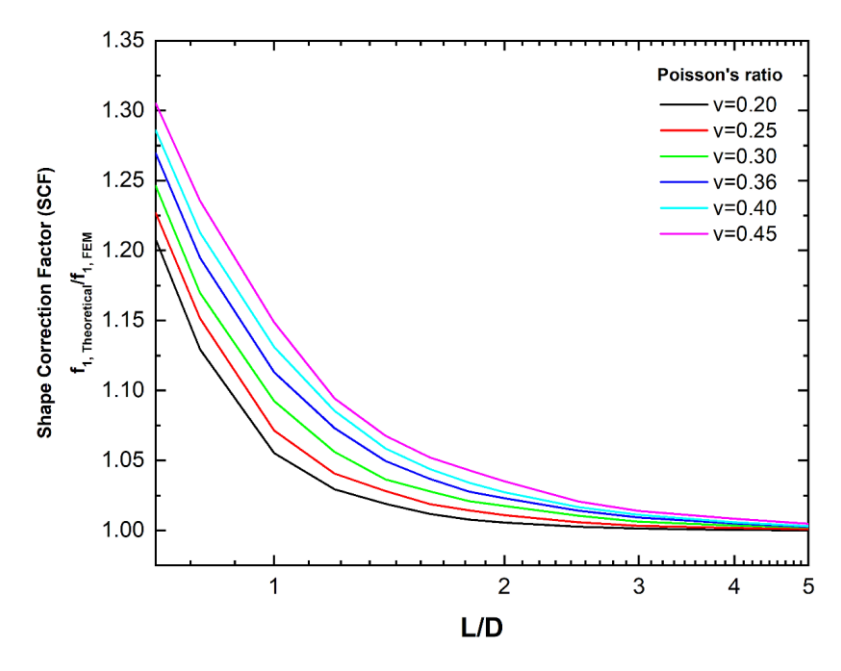


Figure 4. Shape correction factor versus slenderness L/D for six Poisson's ratio values

It becomes obvious that the value of Poisson's ratio must be assumed at the beginning or as a part of a correction factor and then calculated through an iterative process for the optimum value to be obtained. This can be achieved either by two consecutive tests of IE, longitudinal and torsional measurements through Equation 7 or by the combination of two methods, UPV-IE longitudinal tests, through Equations 1, 3, 11, and 12, and UPV and IE torsional tests, through Equations 1, 4, and 14 [32]. The latter has been applied to concrete cores through a new methodology, ultrasonic pulse impact echo synergy (UPIES) [8].

$$v = \frac{E_d - M + S}{4 \cdot M} \tag{12}$$

$$S = \pm \sqrt{E_d^2 + 9M^2 - 10E_dM}$$
 (13)

$$\nu = \frac{{}^{M-2 \cdot G_d}}{{}^{2 \cdot M-2 \cdot G_d}} \tag{14}$$

Therefore, in this study, an experimental evaluation of the proposed SCF on steel and aluminium specimens is conducted. Using FEM analysis, a simulation of the IE method on short cylinders is presented, and the effects of the inertia and mass of the sensor are confirmed. Two new safety factors are proposed on the basis of the FEM results. Finally, a comparison between three methods of Poisson's ratio calculation is presented using UPV and IE tests in combination before conclusions are drawn.

2. Research Methodology

In the present study, experimental evaluation of the SCF for the longitudinal frequency mode was conducted on both steel and aluminum specimens with different slenderness ratios. To cover a wide range of configurations, a total of six distinct slenderness ratios were chosen. The specimens' set is shown in Figure 5. The two materials were selected because of their disparate mechanical characteristics, which provide a thorough foundation for comparison.



Figure 5. Steel and Aluminium cylinders of six different slenderness

The specimens were tested under both longitudinal and torsional impact tests, and the results were corrected by applying the proposed SCF of Siorikis et al. (2020, 2022, 2024) [8, 29, 31], as well as inertia and mass correction factors derived from the following numerical analysis.

2.1. Specimen Properties and Apparatuses

The experimental program was designed to replicate the boundary conditions and loading scenarios used in the FEM simulations of the SCF. Key parameters such as material size and mass as well as the frequency spectra after excitation were recorded and analyzed. The properties of the specimens are shown in Table 1, where W is the weight, L is the length, D is the diameter, γ is the specific weight and ρ is the density of the specimens.

No.	Specimen	W (g)	L (m)	D (m)	$\gamma (kN/m^3)$	$\rho (kg/m^3)$
1	Steel	1968.1	0.20	0.04	76.81	7830.70
2	Steel	1575.4	0.16	0.04	76.86	7835.40
3	Steel	1182.3	0.12	0.04	76.91	7840.37
4	Steel	787.8	0.08	0.04	76.87	7836.39
5	Steel	473.3	0.048	0.04	76.83	7831.99
6	Steel	394.1	0.04	0.04	76.90	7839.38
7	Aluminium	707.4	0.20	0.04	27.61	2814.66
8	Aluminium	565.7	0.16	0.04	27.60	2813.56
9	Aluminium	425.5	0.12	0.04	27.67	2821.35
10	Aluminium	285.3	0.08	0.04	27.90	2796.68
11	Aluminium	171.6	0.048	0.04	27.91	2845.06
12	Aluminium	142.0	0.04	0.04	27.50	2803.97

Table 1. Specimen properties

2.1.1. UPV Test

For the UPV test, the pulse velocity V_p was measured via a Proceq Tico apparatus with a measurement range of -15 to 6550 μ s and a resolution of 0.1 μ s. According to BS 1881: Part 203, typical 54 kHz transducers are not suitable due to the specimens' size and 150 kHz transducer must be used [33]. Proceq Tico is compatible with transducers of such frequency. For this case, ProceqUPV 150 kHz transducers were used with a sensitivity of ± 10 kHz [33]. The apparatus is depicted in Figure 6.



Figure 6. UPV tests on short cylinders

2.1.2. Impact Echo Test

For the IE test, the longitudinal and torsional rod velocities were measured independently via a lightweight Kistler KS94C100 accelerometer with a mass of 4 grams, a sensitivity of 100 mV/g and a frequency range larger than 70 kHz. This IEPE piezoelectric vibration transducer is appropriate for situations where small sensor dimensions are crucial as well as for lightweight measurement devices. Another benefit is their high upper cutoff frequency. Equally high accelerations and, when combined with the right amplifier, very low accelerations can be recorded owing to the incredibly low-noise piezoelectric measurement method. The response of the specimens after excitation in the time domain was recorded. The signals were recorded via the Spider 20HE Digital Signal Analyzer (DSA) of Crystal Instruments with a maximum sampling rate of 512 kHz and a maximum useful bandwidth of 115.2 kHz in any case larger than 20 kHz and a block size of at least 1024 points of the waveform. Its input is individually programmable to accept voltage from an IEPE (ICP) sensor with built-in electronics such as the KS94C100 accelerometer.

The experimental setup is shown in Figure 7. In Figure 8, an example of the frequency spectrum of a steel cylinder specimen with L/D= 4.0 with the first dominant frequency marked is presented. The dominant frequencies are those that were recorded when a waveform analyzer was used; the resonant frequency is the frequency with the highest peak in the amplitude spectrum or the power spectrum obtained from the fast Fourier transform of the recorded accelerometer signal [11].



Figure 7. Impact echo tests on short cylinders

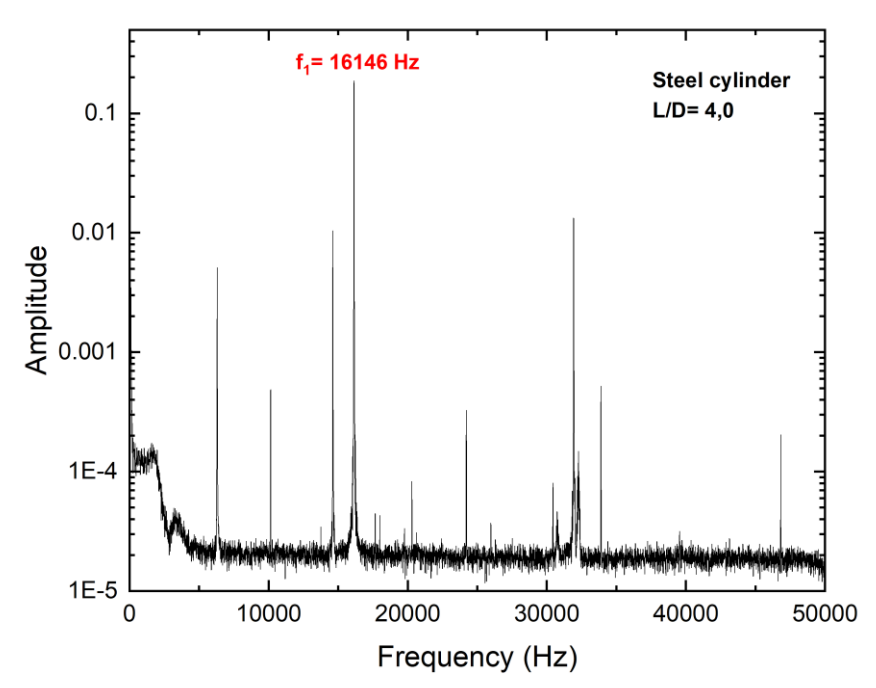


Figure 8. Frequency spectrum of a steel cylinder with a slenderness of L/D= 4.0

2.2. Experimental Evaluation of SCFs

From the measured UPV travel time, the pulse velocity and, consequently, through Equation 1, the constrained modulus, M, can be calculated.

From the first IE test after a longitudinal impact, the measured longitudinal frequencies were corrected via Equations 9 and 10 with a Poisson's ratio of 0.285 for steel and v= 0.341 for aluminium specimens and reference rod velocities of 5155 m/s and 5070 m/s, respectively, on the theoretical basis that from that value, slenderness L/D= 5 and above, the cylinder behaves as an infinite rod. Finally, the results are compared to the curves of the SCF for the corresponding Poisson's ratio values. The specimens were then subjected to a second IE test under torsional impact to measure the torsional frequencies. The frequencies from both the longitudinal and torsional IE tests were then corrected due to the inertia effect and the mass of the accelerometer interaction. The inertia correction factor (ICF) and mass correction factor (MCF) were obtained from extensive numerical analysis.

Finally, using the pulse velocity V_p , the corrected values of the longitudinal rod velocity V_c , shear velocity V_s , and Poisson's ratio are calculated via three procedures:

By IE (longitudinal) and IE (torsional) tests through Equation 7.

By UPV and IE (longitudinal) tests through Equation 12.

By UPV and IE (torsional) tests through Equations 5 to 7.

All the procedures required two independent tests. The first differs in that only the IE method was used yet again, with two implementations.

2.3. Numerical Investigation

The finite element method (FEM) is a powerful computational tool widely used in civil engineering, offering numerous advantages for solving complex problems in structural analysis, design, and material behavior. In recent years, researchers have used FEM analysis to simulate the IE method on cylinders to estimate the dynamic properties of materials [8, 29, 31, 34]. Slenderness of the specimen and mass of the sensor are among the parameters that affect the results. Since the specimen's mass (W) to the accelerometer's mass (W_0) ratio is considerably small for certain specimens, a numerical investigation is essential to assess the effect of the partially attached mass on a specimen when V_c and V_s are determined from the IE test. In this context, a total of 24 simulations were conducted to determine the required corrections to the measured frequencies. The software used for the abovementioned simulations is Plaxis 3D from Bentley Systems.

In this investigation, the IE test under both longitudinal and torsional impact was simulated for steel and aluminum specimens, as shown in Figure 9. The material of the simulated specimens was modeled as linear elastic, with V_p = 5910 m/s and V_p = 6410 m/s for the steel and aluminium models, respectively. Poisson's ratios of v= 0.285 and v= 0.341 were applied for the steel and aluminium models, respectively. The specific weights of the simulated materials were set to match those of the original specimens, as listed in Table 1. The accelerometer was modeled as a cylinder with a diameter of 10 mm and a height of 8 mm, with a specific weight of γ = 46.84 kN/m³, resulting in an accelerometer mass of W_o = 3 g, which was the mass of the accelerometer used in the IE tests.

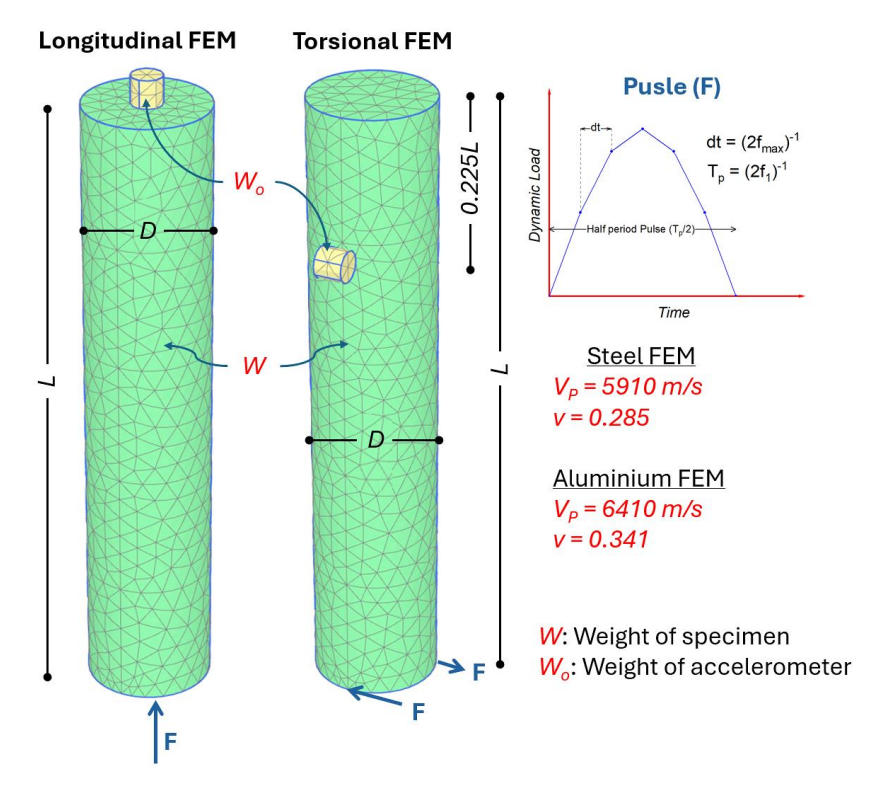


Figure 9. Finite element modeling in PLAXIS 3D for simulating longitudinal and torsional IE tests under longitudinal and torsional impact

The mesh density was set to approximately 16 elements per square centimeter. Dynamic excitations were applied as half-period pulse loads parallel to the axis of the specimen for the longitudinal models and as a pair of half-period pulse forces applied transverse to the axis of the specimen for the torsional models, as shown in Figure 9. The frequency is equal to half of the expected dominant eigenfrequency, f_1 . The time increment between the steps in the analysis was selected to ensure that the maximum frequency captured was at least f_{max} =3 f_1 . For model validation, dynamic analyses were performed on reference FEM specimens without the accelerometer's mass, and the results were compared with analytical solutions. To minimize the error between the reference FEM results and the analytical solutions, each time increment was divided into at least 10 substeps.

The properties of the finite element model (FEM) used for the simulation of both longitudinal and torsional IE tests are presented in Table 2.

Table 2. Specimen properties as modeled in PLAXIS 3D for IE test simulations under longitudinal and torsional impact

No.	Specimen	W (gr)	$W_{o}\left(gr\right)$	L (m)	D (m)	L/D	W/W _o
1	Steel	1968.1	3.0	0.20	0.04	5.0	656.0
2	Steel	1575.4	3.0	0.16	0.04	4.0	525.1
3	Steel	1182.3	3.0	0.12	0.04	3.0	394.1
4	Steel	787.8	3.0	0.08	0.04	2.0	262.6
5	Steel	473.3	3.0	0.048	0.04	1.2	157.8
6	Steel	394.1	3.0	0.04	0.04	1	131.4
7	Aluminium	707.4	3.0	0.20	0.04	5.0	235.8
8	Aluminium	565.7	3.0	0.16	0.04	4.0	188.6
9	Aluminium	425.5	3.0	0.12	0.04	3.0	141.8
10	Aluminium	285.3	3.0	0.08	0.04	2.0	95.1
11	Aluminium	171.6	3.0	0.048	0.04	1.2	57.2
12	Aluminium	142.0	3.0	0.04	0.04	27.50	2803.97

The correction factor for the longitudinal IE tests is determined by the mass correction factor (MCF) from Equation 15, whereas the correction factor for the torsional IE tests is given by the inertia correction factor (ICF) from Equation 16.

$$MCF = \frac{f_L}{f_{Lmass}} \tag{15}$$

$$ICF = \frac{f_T}{f_{T,mass}} \tag{16}$$

where f_L and $f_{L,mass}$ represent the frequencies obtained from FEM simulations of the longitudinal IE test, without and with the accelerometer mass, respectively, and where f_T and $f_{T,mass}$ correspond to the frequencies obtained from the torsional IE test, with and without the accelerometer mass, respectively.

3. Results and Discussion

3.1. Numerical Results-Inertia & Mass Correction Factors

The dynamic analysis of the IE test simulations, both with and without the mass of the accelerometer, indicates that corrections must be applied to the measured longitudinal frequencies when the accelerometer mass is included to align them with the frequencies obtained without the mass. When the W/W_0 ratio is lower than 200, the MCF should be applied. For high values of the W/W_0 ratio, this MCF seems to have no significant influence, as for a value of approximately 600, which is approximately the same as a typical drilled concrete or rock core with L/D=1, the corresponding correction is approximately 3.5%. Thus, taking into account only the mass of the sensor effect, IE can be applied without any correction to the longitudinal or torsional frequencies of the concrete cores.

Slenderness had no effect on the IE test results under torsional impact; therefore, no shape correction was applied. Inertia, on the other hand, plays a significant role, especially for small slenderness, and the ICF has to be applied. In Table 3, the results of the MCF and ICF are presented for the 12 FEM specimens of steel and aluminium obtained from longitudinal and torsional IE test simulations, respectively. In Figure 10, the mass correction factor (MCF) results for the steel and aluminium FEM specimens, obtained from FEM impact echo (IE) tests under longitudinal impact with and without accounting for the accelerometer mass versus the specimento-accelerometer mass ratio (W/W $_0$) can be seen, whereas in Figure 11, the inertia correction factor (ICF) results for the steel and aluminium FEM specimens, obtained from FEM Impact Echo (IE) tests under torsional impact with and without accounting for the accelerometer mass, versus the specimen-to-accelerometer mass ratio (W/W $_0$) is illustrated.

Table 3. MCF and ICF results from IE test numerical simulations under longitudinal and torsional impact

No.	Specimen	L/D	W/W_0	MCF	ICF
1	Steel	5.0	656.0	1.0035	1.0008
2	Steel	4.0	525.1	1.0042	1.0009
3	Steel	3.0	394.1	1.0045	1.0012
4	Steel	2.0	262.6	1.0068	1.0015
5	Steel	1.2	157.8	1.0096	1.0041
6	Steel	1	131.4	1.0120	1.0072
7	Aluminium	5.0	235.8	1.0075	1.0091
8	Aluminium	4.0	188.6	1.0083	1.0091
9	Aluminium	3.0	141.8	1.0110	1.0109
10	Aluminium	2.0	95.1	1.0136	1.0136
11	Aluminium	1.2	57.2	1.0214	1.0233
12	Aluminium	27.50	2803.97	1.0297	1.0347

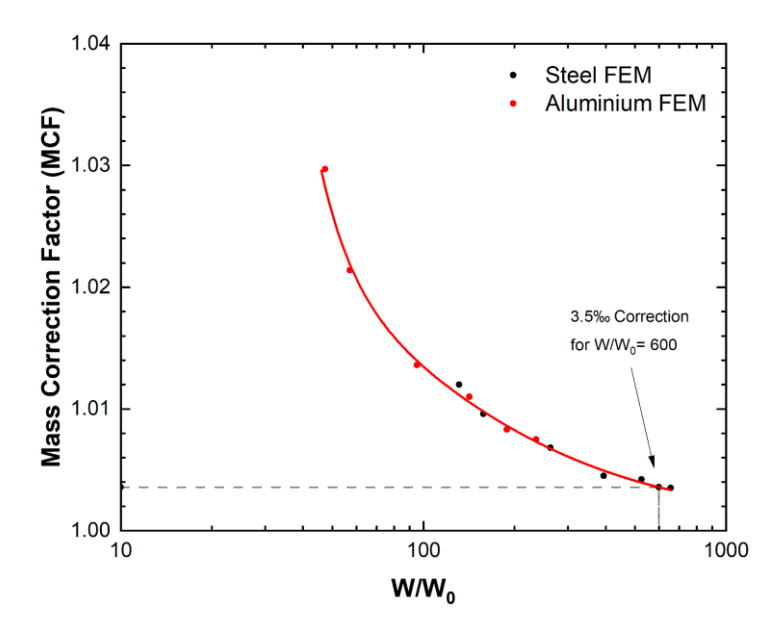


Figure 10. Mass correction factor (MCF) results for steel and aluminium FEM specimens under longitudinal impact versus the mass of specimen to mass ratio of the accelerometer (W/W_0)

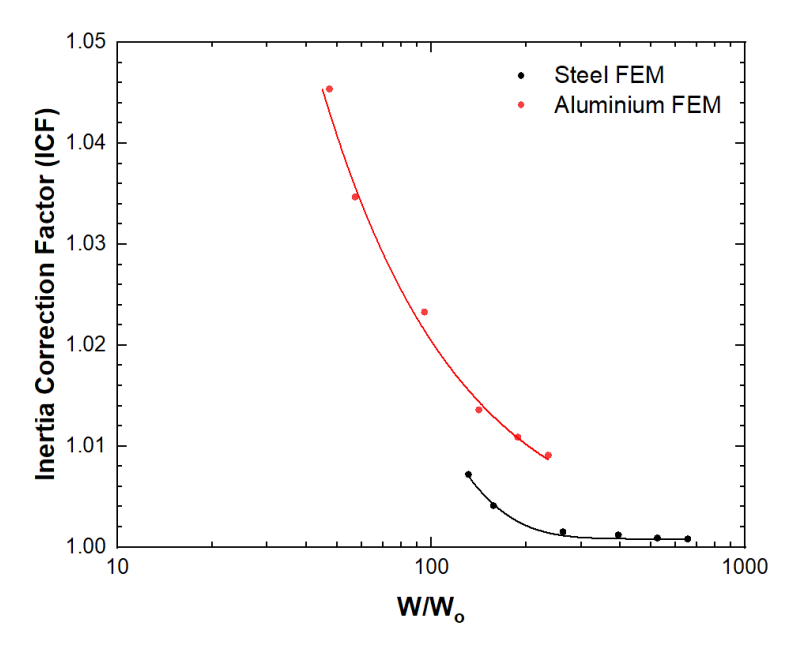


Figure 11. Inertia correction factor (ICF) results for the steel and aluminium FEM specimens under torsional impact versus the mass of specimen to mass ratio of the accelerometer (W/W_0)

3.2. Experimental Evaluation of SCFs

3.2.1. UPV Results

Table 4 shows the results after the 12 specimens were tested via the UPV method. The 3^{rd} column shows the slenderness of the specimen L/D, the 4^{th} column shows the pulse travel time in μs , the 5th column shows the calculated pulse velocity in m/s, and the 6th column shows the calculated constrained modulus and average value in column 7.

Table 4. UPV Results

No.	Specimen	L/D	t _p (µs)	V _p (m/s)	M (GPa)	M _{aver} (GPa)
1	Steel	5	34.0	5882	270.96	
2	Steel	4	27.1	5904	273.13	
3	Steel	3	20.3	5911	273.97	272.02
4	Steel	2	13.7	5926	275.19	273.93
5	Steel	1.2	8.1	5926	275.03	
6	Steel	1	6.8	5926	275.29	
7	Aluminium	5	31.70	6310	114.19	
8	Aluminium	4	25.10	6349	115.04	
9	Aluminium	3	18.90	6443	113.36	115.79
10	Aluminium	2	12.60	6486	116.09	113.79
11	Aluminium	1.2	7.40	6441	119.70	
12	Aluminium	1	6.21	6369	116.33	

3.2.2. IE Results-Longitudinal Mode

The experimental results confirmed the need to use an SCF for the longitudinal mode, whereas the MCF retrieved from the numerical analysis revealed that the mass of the accelerometer interaction with the mass of the specimen was significant and cannot be ignored. Figures 12 and 13 show the experimental results for steel and aluminium cylinders with six different slenderness values with SCF and MCF and without correction. The deviation is notable, whereas the plotted curves for Poisson's ratio v= 0.285 for steel and v= 0.341, which are in line with the results, confirm the need for shape and mass correction on the measured frequencies. The dynamic Young's modulus was calculated on the basis of the corrected frequencies/longitudinal velocities. In Table 5, the results for the 12 specimens subjected to longitudinal impact can be seen where the 3rd column is the slenderness of the specimen L/D, the 4th column is the mass of specimen to the mass of the accelerometer ratio, the 5th column is the measured longitudinal resonant frequency in Hz, the 6th column is the SCF, the 7th column is the MCF derived from the FEM curve in the 8th column is the final correction factor, the 9th column is the corrected rod velocity, the 10th column is the ratio of the rod velocity to the UPV velocity ratio, and the 11th column is the calculated dynamic Young's modulus and their average value in column 12.

Table 5. IE longitudinal results

No.	Specimen	L/D	W/W ₀	f _{cm} (Hz)	SCF	MCF	Final Correction	Vc cor (m/s)	Vc/Vp	E (GPa)	E _{aver} (GPa)
1	Steel	5	492.0	12931	0.99777	1.00333	1.00109	5178	0.88027	209.96	
2	Steel	4	393.9	16146	0.99886	1.00395	1.00281	5181	0.87757	210.35	
3	Steel	3	295.6	21485	1.00367	1.00493	1.00862	5186	0.87735	210.89	211.40
4	Steel	2	197.0	31310	1.00956	1.00674	1.01636	5196	0.87676	211.54	211.49
5	Steel	1.2	118.3	51400	1.04998	1.00979	1.06027	5211	0.87943	212.71	
6	Steel	1	98.5	59900	1.07697	1.01114	1.08897	5218	0.88060	213.48	
7	Aluminium	5	176.9	12775	0.99424	1.00731	1.00151	5118	0.80348	205.09	
8	Aluminium	4	141.4	15900	0.99542	1.00862	1.00401	5124	0.80138	205.75	
9	Aluminium	3	106.4	21300	0.99551	1.01056	1.00602	5134	0.80999	206.67	209.42
10	Aluminium	2	71.3	31100	1.00617	1.01397	1.02023	5152	0.79957	207.97	208.42
11	Aluminium	1.2	42.9	50432	1.04938	1.02186	1.07232	5192	0.80038	211.10	
12	Aluminium	1	35.5	59900	1.08329	1.02825	1.11390	5224	0.81104	213.95	

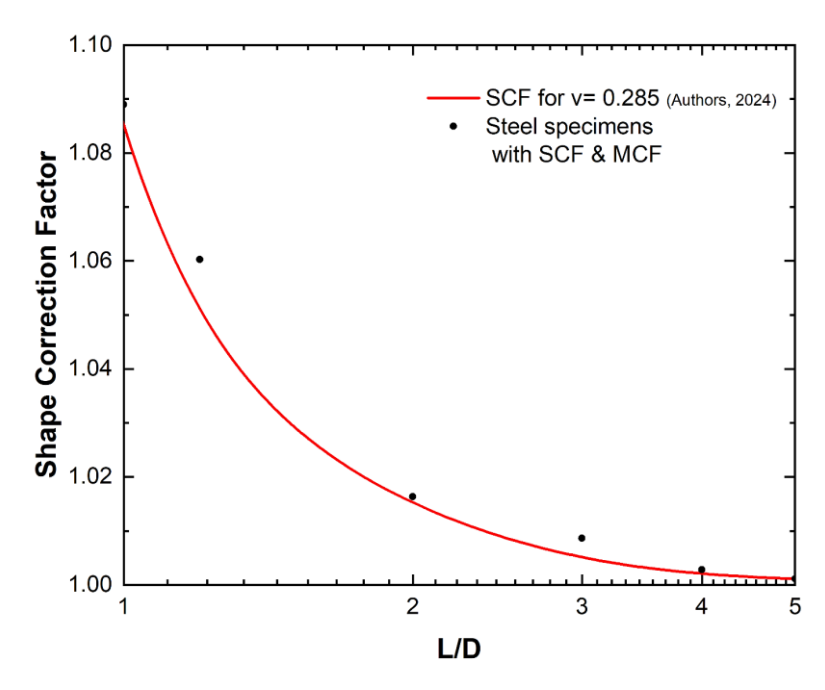


Figure 12. Experimental results for steel cylinders with six different slenderness values versus the SCF

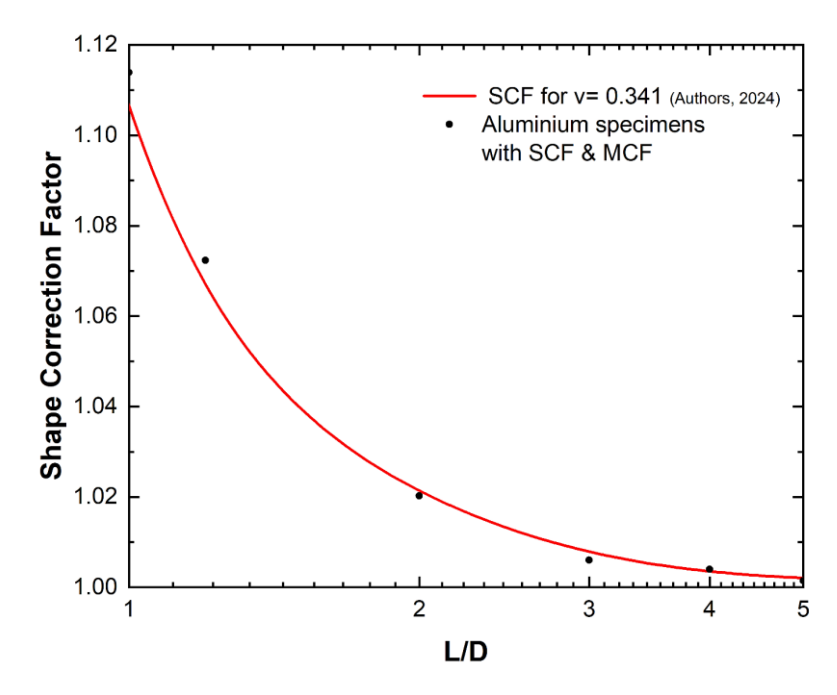


Figure 13. Experimental results for aluminum cylinders with six different slenderness values versus SCF

3.2.3. IE Results-Torsional Mode

The experimental results were corrected with the ICF. Through the corrected torsional frequencies/velocities, the dynamic shear modulus of the specimens was calculated. In Table 6, the results for the 12 specimens of steel and aluminium when tested under longitudinal impact can be seen where the 3rd column is the slenderness of the specimen L/D, the 4th column is the measured torsional resonant frequency in Hz, the 5th column is the inertia correction factor ICF derived from the FEM curve, the 6th column is the corrected torsional velocity, the 7th column is the torsional-to-UPV velocity ratio, and the 8th column is the calculated dynamic Young's modulus from Equation 1 and their average value on column 9.

Table 6. IE Torsional Results

No.	Specimen	L/D	f _{sm} (Hz)	ICF	Vs cor (m/s)	Vs/Vp	G (GPa)	Gaver (GPa)
1	Steel	5	8075	1	3230	0.5491	81.70	
2	Steel	4	10100	1	3232	0.54742	81.85	
3	Steel	3	13475	1	3234	0.547085	82.00	02.27
4	Steel	2	20250	1	3240	0.54675	82.26	82.27
5	Steel	1.2	33725	1.004	3251	0.54853	82.75	
6	Steel	1	40398	1.007	3254	0.549191	83.03	
7	Aluminium	5	7740	1.008652248	3123	0.490277615	76.36	
8	Aluminium	4	9640	1.010819516	3128	0.489163867	76.66	
9	Aluminium	3	12850	1.014386179	3123	0.492717799	76.48	77.72
10	Aluminium	2	19010	1.021453207	3153	0.489329202	77.89	77.73
11	Aluminium	1.2	31940	1.035665754	3176	0.48957163	78.98	
12	Aluminium	1	38285	1.043102817	3195	0.495995077	80.02	

3.3. Poisson's Ratio Calculation

With the three moduli already calculated and using the equations described in the Methodology section, Poisson's ratio was calculated. Table 7 shows the individual calculations for all the specimens as well as the average values of the two materials. The three methods were compared, and it is evident that the error in the Poisson's ratio calculation when no correction factors are applied is significant. Figure 14 shows a Poisson's ratio comparison of steel cylinders versus slenderness for three different test combinations, without accounting for the MCF in the IE test under longitudinal impact (used for calculating E_d) and the ICF under torsional impact (used for calculating G_d), whereas Figure 16 shows the same Poisson's ratio calculation for aluminium. Figure 15 shows a comparison of the Poisson's ratio for steel cylinders versus slenderness for three different test combinations, accounting for the MCF in the IE test under longitudinal impact (used for calculating E_d) and the ICF under torsional impact (used for calculating E_d), and Figure 17 shows the same results for aluminium cylinders. Their individual values have a very good distribution around the average.

Table 7. Poisson's ratio calculation

No.	Specimen	$M - E_d$	M - G_d	E_d - G_d
1	Steel	0.284	0.284	0.285
2	Steel	0.286	0.286	0.285
3	Steel	0.287	0.286	0.286
4	Steel	0.287	0.287	0.286
5	Steel	0.285	0.285	0.285
6	Steel	0.284	0.284	0.286
	Average	0.285	0.285	0.285
7	Aluminium	0.342	0.342	0.343
8	Aluminium	0.343	0.343	0.342
9	Aluminium	0.338	0.340	0.351
10	Aluminium	0.344	0.343	0.335
11	Aluminium	0.343	0.342	0.336
12	Aluminium	0.337	0.337	0.337
	Average	0.341	0.341	0.341

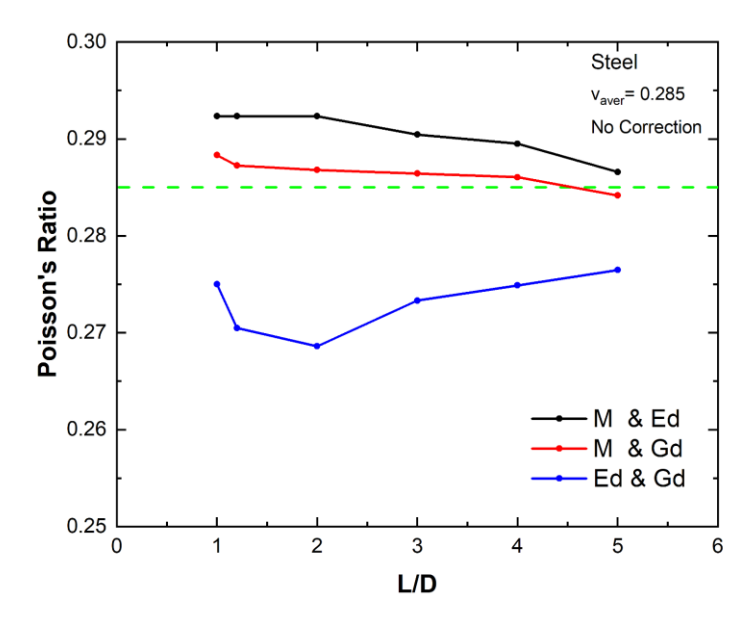


Figure 14. Poisson's ratio comparison of steel cylinders and slenderness for three different test combinations without correction

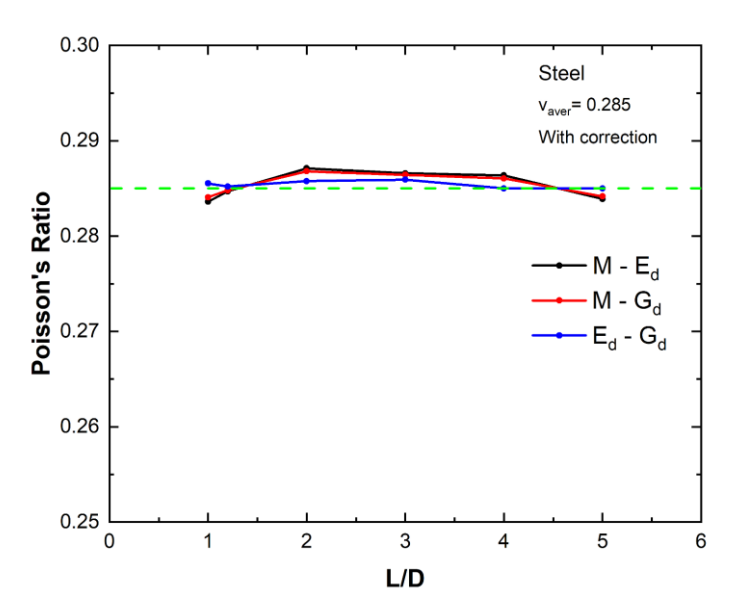


Figure 15. Poisson's ratio comparison of steel cylinders and slenderness for three different test combinations with correction

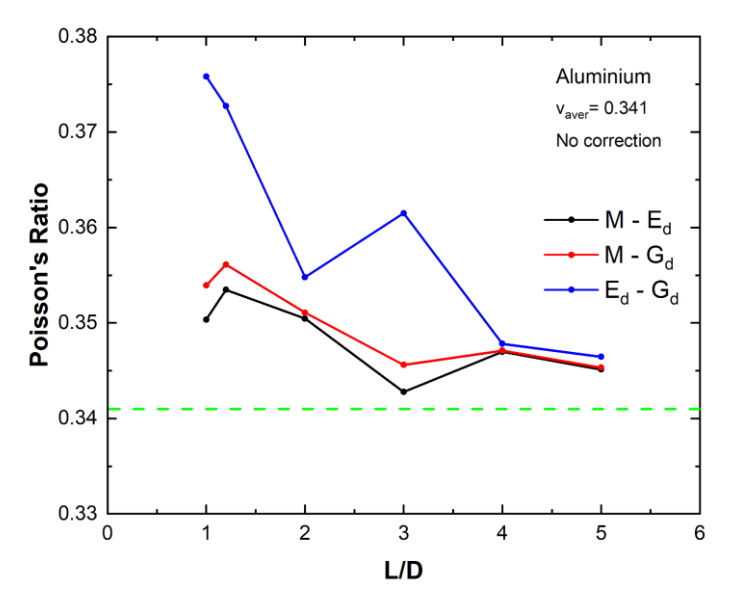


Figure 16. Poisson's ratio comparison of aluminium cylinders and slenderness for three different test combinations without correction

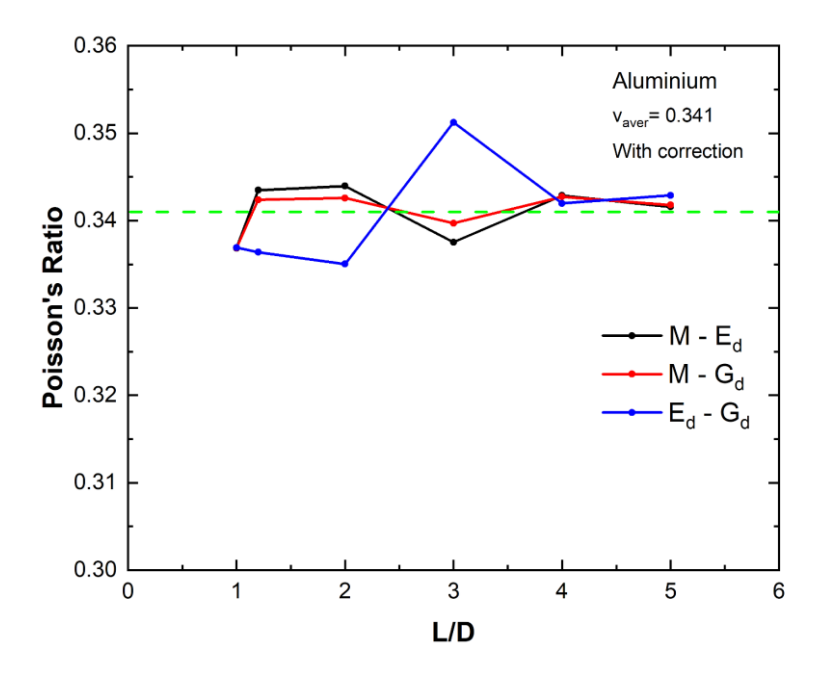


Figure 17. Poisson's ratio comparison of aluminum cylinders and slenderness for three different test combinations with correction

Figure 18 illustrates a theoretical example of the Poisson's ratio error versus the Poisson's ratio obtained from the three different test combinations (M- E_d , M- G_d and E_d - G_d) when the error in the measured velocity ratio of the three test combinations, V_p/V_c , V_p/V_s and V_c/V_s , is 1%. The most unreliable seems to be the IE for the longitudinal and torsional tests, as a large fluctuation in the true Poisson's ratio results in approximately the same error, especially if we narrow the range of the Poisson's ratio between 0.25 and 0.35, where the true Poisson's ratio value is uncertain. The other two methods are quite similar for high Poisson's ratio values, but when again, if we focus on the abovementioned range, the combination of UPV and the longitudinal mode of IE yields more reliable results.

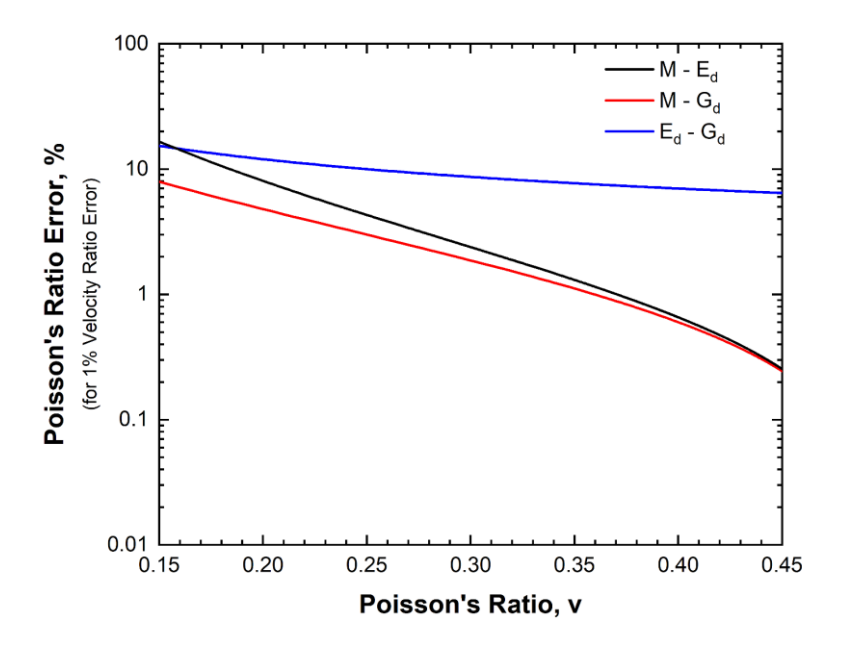


Figure 18. Example of the Poisson's ratio error versus the Poisson's ratio from the three different test combinations when the error in the measured velocity ratio is 1%

To determine the dynamic properties of short cylinders, the combination of two independent tests, a UPV and an IE in longitudinal mode, is a more reliable approach. When testing steel and aluminium cylinders, the slenderness effect must be considered. The mass of the sensor adds to the results as well. The measured frequencies must be corrected via SCF and MSC. For concrete cylinders, the frequencies must be corrected because of the slenderness effect, but due to the large W/W_0 ratio, no mass correction is necessary. A flowchart of the methodology is shown in Figure 19.

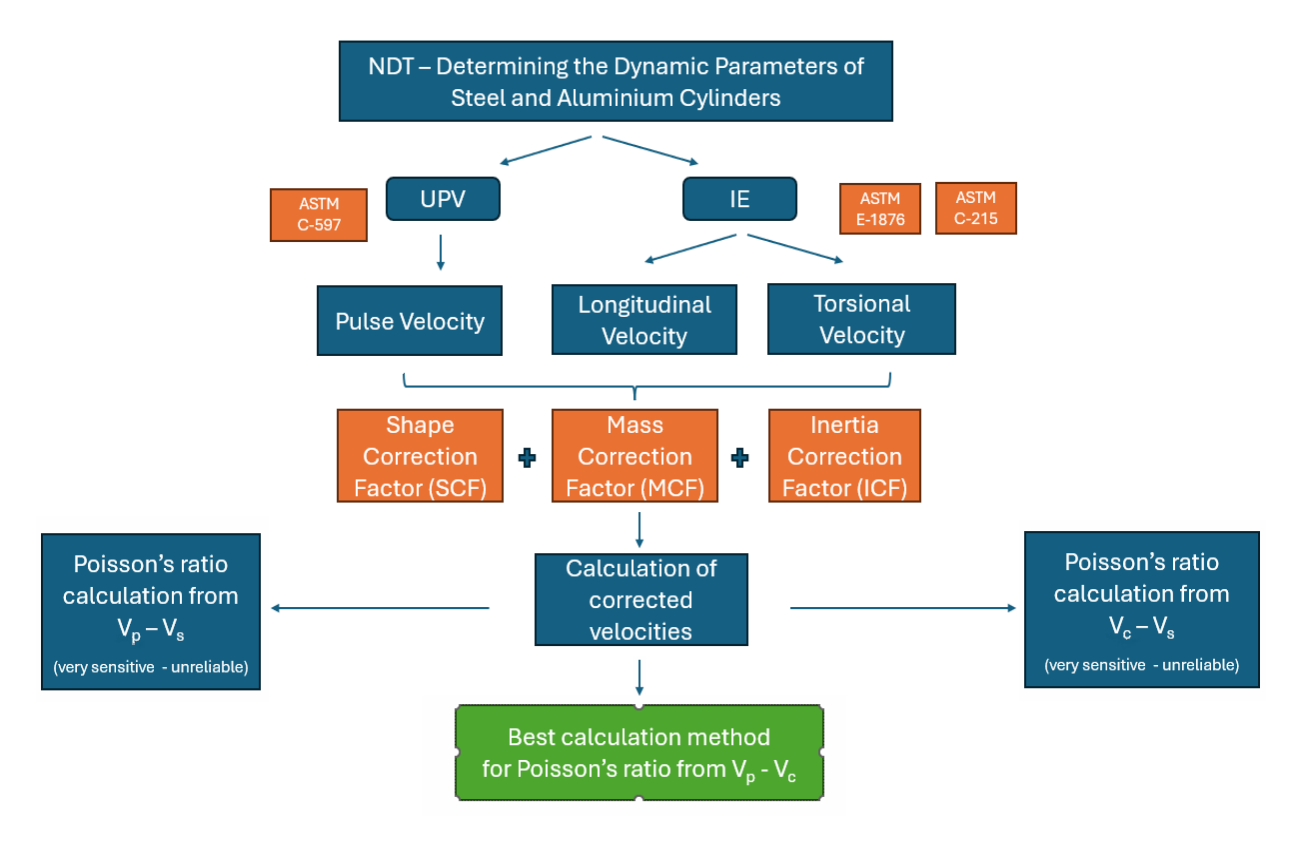


Figure 19. Flowchart of Poisson's ratio calculation using the proposed CF

4. Conclusions

This research focuses on the determination of the dynamic parameters of short cylinders via an increasingly widely used NDT method, impact echo (IE), through experimental and numerical analysis. Twelve cylindrical specimens, six made of steel and six made of aluminium, were tested via the UPV and IE methods. The pulse, rod and torsional velocities were calculated through their corresponding measured frequencies and corrected via the shape correction factor SCF. Twenty-four FEM simulations in Plaxis 3D showed that the inertia effect and the mass of the accelerometer interaction with the mass of the cylinder significantly affect the results. Specifically, slenderness affects the results in the longitudinal mode but does not affect the torsional mode. In contrast, mass and inertia affect both modes, especially the lower slenderness and lower mass of the specimen to mass of the sensor ratio. Two new correction factors, MCF and ICF, were proposed for mass and inertia correction, respectively. Three different combination methods were tested for Poisson's ratio calculation. By comparing the experimental outcomes with FEM predictions, the reliability and limitations of the numerical model are critically evaluated, offering insight into its applicability for different slenderness and material combinations.

The integration of the UPV and IE in longitudinal mode appears to be the optimal solution for determining the most reliable approach for calculating Poisson's ratio. This calculation for short cylinders is affected by slenderness, but it is also very sensitive to small changes in mass and inertia. For the tested materials with various parameters of slenderness and mass, the Poisson's ratio can be accurately calculated. For typical concrete and rock cores with a slenderness of L/D=1, no significant effect on the Poisson's ratio is observed because of the large mass of the specimen to mass of the sensor ratio (W/W₀). For W/W₀<200, the MCF and ICF must be applied. The MCF and ICF obtained from the numerical investigation are intended for use only in correcting the specimens of this study. Further investigations are needed to determine the correction factors that can be applied universally. Furthermore, replacing the accelerometer with an interferometer eliminates the need for mass correction. In conclusion:

- The dynamic moduli can be determined via the UPV and IE.
- The results must be corrected by applying a CF for slenderness, mass and inertia.
- Poisson's ratio was accurately calculated for the steel and aluminium specimens of the present study.
- Poisson's ratio can be calculated for concrete and rock cores with L/D=1 because of the large W/W₀.
- UPV in combination with IE in longitudinal mode is the most reliable method for Poisson's ratio calculation.

5. Declarations

5.1. Author Contributions

Conceptualization, P.P. and V.G.S.; methodology, P.P.; software, P.P.; validation, P.P., K.P.A., and G.D.H.; formal analysis, P.P. and V.G.S.; investigation, P.P., V.G.S., and K.P.A.; resources, P.P. and K.P.A.; data curation, P.P., K.P.A., and V.G.S.; writing—original draft preparation, V.G.S.; writing—review and editing, P.P.; visualization, V.G.S. and P.P.; supervision, P.P.; project administration, P.P. and V.G.S.; funding acquisition, P.P. All the authors have read and agreed to the published version of the manuscript.

5.2. Data Availability Statement

The data presented in this study are available upon request from the corresponding author.

5.3. Funding and Acknowledgments

The authors acknowledge financial support for the dissemination of this work from the Special Account for Research of ASPETE through the funding program "Strengthening ASPETE's research.

5.4. Conflicts of Interest

The authors declare no conflict of interest.

6. References

- ASTM C597-16. (2023). Standard Test Method for Pulse Velocity through Concrete. ASTM International, Pennsylvania, United States. doi:10.1520/C0597-16
- [2] Panzera, T. H., Christoforo, A. L., de Paiva Cota, F., Ribeiro Borges, P. H., & Bowen, C. R. (2011). Ultrasonic Pulse Velocity Evaluation of Cementitious Materials. Advances in Composite Materials Analysis of Natural and Man-Made Materials, IntechOpen Limited, London, United Kingdom. doi:10.5772/17167.
- [3] Hobbs, B., & Tchoketch Kebir, M. (2007). Non-destructive testing techniques for the forensic engineering investigation of reinforced concrete buildings. Forensic Science International, 167(2–3), 167–172. doi:10.1016/j.forsciint.2006.06.065.
- [4] Turgut, P. (2004). Evaluation of the ultrasonic pulse velocity data coming on the field. 4th International Conference on NDE in relation to Structural Integrity for Nuclear and Pressurised Components, 6-8 December, 2004, London, United Kingdom.
- [5] Trtnik, G., Kavčič, F., & Turk, G. (2009). Prediction of concrete strength using ultrasonic pulse velocity and artificial neural networks. Ultrasonics, 49(1), 53–60. doi:10.1016/j.ultras.2008.05.001.
- [6] Diaferio, M., & Vitti, M. (2020). Correlation Curves to Characterize Concrete Strength by Means of UPV Tests. Proceedings of 1st International Conference on Structural Damage Modelling and Assessment, 4–5, August, 2020, Ghent University, Ghent, Belgium. doi:10.1007/978-981-15-9121-1_16.
- [7] Choi, Y., Kim, I. H., Lim, H. J., & Cho, C. G. (2022). Article Investigation of Strength Properties for Concrete Containing Fine-Rubber Particles Using UPV. Materials, 15(10), 3452. doi:10.3390/ma15103452.
- [8] Siorikis, V. G., Antonopoulos, C. P., Pelekis, P., Christovasili, K., & Hatzigeorgiou, G. D. (2020). Numerical and experimental evaluation of sonic resonance against ultrasonic pulse velocity and compression tests on concrete core samples. Vibroengineering Procedia, 30, 168–173. doi:10.21595/vp.2020.21328.
- [9] Espinosa, A. B., Revilla-Cuesta, V., Skaf, M., Faleschini, F., & Ortega-López, V. (2023). Utility of Ultrasonic Pulse Velocity for Estimating the Overall Mechanical Behavior of Recycled Aggregate Self-Compacting Concrete. Applied Sciences, 13(2), 874. doi:10.3390/app13020874.
- [10] ASTM E1876-22. (2022). Standard Test Method for Dynamic Young's Modulus, Shear Modulus, and Poisson's Ratio by Impulse Excitation of Vibration. ASTM International, Pennsylvania, United States. doi:10.1520/E1876-22.
- [11] ASTM C215-19. (2020). Standard Test Method for Fundamental Transverse, Longitudinal, and Torsional Resonant Frequencies of Concrete Specimens. ASTM International, Pennsylvania, United States. doi:10.1520/C0215-19.
- [12] Coleman, Z. W., & Schindler, A. K. (2025). Investigation of Ground-Penetrating Radar, Impact Echo, and Infrared Thermography Methods to Detect Defects in Concrete Bridge Decks. Transportation Research Record, 2679(1), 169–182. doi:10.1177/03611981221101027.
- [13] Thurnherr, C., Muller, A., & Algernon, D. (2025). Drone-based impact-echo inspection system for non-destructive testing of concrete structures. Construction and Building Materials, 477. doi:10.1016/j.conbuildmat.2025.141147.
- [14] Yoon, Y. G., Kim, C. M., & Oh, T. K. (2022). A Study on the Applicability of the Impact-Echo Test Using Semi-Supervised Learning Based on Dynamic Preconditions. Sensors, 22(15), 5484. doi:10.3390/s22155484.

- [15] Bahati, P. A., Le, V. D., & Lim, Y. (2021). An impact echo method to detect cavities between railway track slabs and soil foundation. Journal of Engineering and Applied Science, 68(1), 7. doi:10.1186/s44147-021-00008-w.
- [16] Sansalone, M. (1997). Impact-echo: The complete story. ACI Structural Journal, 94(6), 777–786. doi:10.14359/9737.
- [17] Qasrawi, H. Y. (2000). Concrete strength by combined nondestructive methods simply and reliably predicted. Cement and Concrete Research, 30(5), 739–746. doi:10.1016/S0008-8846(00)00226-X.
- [18] Medina, R., & Bayón, A. (2010). Elastic constants of a plate from impact-echo resonance and Rayleigh wave velocity. Journal of Sound and Vibration, 329(11), 2114–2126. doi:10.1016/j.jsv.2009.12.026.
- [19] Nieves, F. J., Gascón, F., & Bayón, A. (2003). Measurement of the dynamic elastic constants of short isotropic cylinders. Journal of Sound and Vibration, 265(5), 917–933. doi:10.1016/S0022-460X(02)01563-8.
- [20] Lee, K.-M., Kim, D.-S., & Kim, J.-S. (1997). Determination of dynamic Young's modulus of concrete at early ages by impact resonance test. KSCE Journal of Civil Engineering, 1(1), 11–18. doi:10.1007/bf02830459.
- [21] Kheder, G. F. (1999). A two stage procedure for assessment of in situ concrete strength using combined non-destructive testing. Materials and Structures, 32(6), 410–417. doi:10.1007/bf02482712.
- [22] Nieves, F. J., Gascón, F., & Bayón, A. (2000). Precise and direct determination of the elastic constants of a cylinder with a length equal to its diameter. Review of Scientific Instruments, 71(6), 2433–2439. doi:10.1063/1.1150632.
- [23] Malone, C., Sun, H., & Zhu, J. (2023). Nonlinear Impact-Echo Test for Quantitative Evaluation of ASR Damage in Concrete. Journal of Nondestructive Evaluation, 42(4), 93. doi:10.1007/s10921-023-01003-2.
- [24] Pandum, J., Hashimoto, K., Sugiyama, T., & Yodsudjai, W. (2024). Impact-Echo for Crack Detection in Concrete with Artificial Intelligence based on Supervised Deep Learning. E-Journal of Nondestructive Testing, 29(6), 1-8. doi:10.58286/29925.
- [25] ASTM C1383-15(2022). (2024). Standard Test Method for Measuring the P-Wave Speed and the Thickness of Concrete Plates Using the Impact-Echo Method. ASTM International, Pennsylvania, United States. doi:10.1520/C1383-15R22
- [26] Love, A. E. H. (1944). A treatise on the mathematical theory of elasticity. Courier Corporation, Chelmsford, United States.
- [27] Dethof, F., & Keßler, S. (2024). Explaining impact echo geometry effects using modal analysis theory and numerical simulations. NDT and E International, 143. doi:10.1016/j.ndteint.2023.103035.
- [28] Yao, F., Zhuang, J., & Abulikemu, A. (2022). Shape coefficient of impact-echo for small-size short cylinder/circular tube structures. Materialpruefung/Materials Testing, 64(4), 574–583. doi:10.1515/mt-2021-2043.
- [29] Siorikis, V. G., Pelekis, P., Antonopoulos, C. P., & Hatzigeorgiou, G. D. (2022). Shape correction factors for impact-echo method on short cylinders: A numerical and experimental study. Proceedings of the 13th HSTAM International Congress on Mechanics. Hellenic Society for Theoretical and Applied Mechanics (HSTAM), Patras, Greece.
- [30] Wang, J. J., Chang, T. P., Chen, B. T., & Wang, H. (2012). Determination of Poissons ratio of solid circular rods by impact-echo method. Journal of Sound and Vibration, 331(5), 1059–1067. doi:10.1016/j.jsv.2011.10.030.
- [31] Siorikis, V. G., Antonopoulos, C. P., Hatzigeorgiou, G. D., & Pelekis, P. (2024). Comparative Study of UPV and IE Results on Concrete Cores from Existing Structures. Civil Engineering Journal, 10(9), 2804–2819. doi:10.28991/cej-2024-010-09-03.
- [32] Mavko, G., Mukerji, T., & Dvorkin, J. (2020). The rock physics handbook. Cambridge University Press, Cambridge, United Kingdom. doi:10.1017/9781108333016.
- [33] BS 1881-203:1986. (1986). The Standard for Testing concrete Recommendations for measurement of velocity of ultrasonic pulses in concrete. British Standard Institute (BSI), London, United Kingdom.
- [34] Pelekis, P., Siorikis, V. G., Antonopoulos, C. P., & Hatzigeorgiou, G. D. (2022). Determination of dynamic elastic properties on short cylinders using impact-echo method: A numerical study. Proceedings of the 13th HSTAM International Congress on Mechanics, Hellenic Society for Theoretical and Applied Mechanics (HSTAM), Patras, Greece.